Neural Computing and Applications
https://doi.org/10.1007/s00521-021-05891-1

ORIGINAL ARTICLE

Analytical approach-based optimization of the actively driven rotary turning for environmental and economic metrics considering energy footprint of materials

Trung-Thanh Nguyen[1]

Received: 1 September 2020 / Accepted: 26 February 2021

Abstract
The current work has been performed an effective optimization to decrease the total energy consumption (E_{total}) and total machining time (T_{total}) with the constraint of the average roughness for the actively driven rotary turning (ADRT) of the material labeled SKD11. The optimizing factors are the tool rotational speed (v_t), depth of cut (a), feed rate (f), and workpiece speed (v_w). The analytical approach was used to construct the models of the E_{total} and T_{total}. The weightage principal component analysis (WPCA) was applied in conjunction with the non-dominated sorting particle swarm optimization (NSPSO) and the Technique for Order of Preference by Similarity to Ideal Solution (TOPSIS) to determine the weight values of machining responses and select the best optimal solution. The scientific findings revealed that the optimal values of the v_t, a, f, and v_w were 78 m/min, 0.21 mm, 0.44 mm/rev., and 98 m/min, respectively. The reductions in the E_{total} and T_{total} were 16.99% and 17.78%, respectively. Moreover, the proposed models of the E_{total} and T_{total} were significant and could be used to predict technical performances with acceptable accuracy. The optimization technique comprising the analytical method, NSPSO, WPCA, and TOPSIS was named as a powerful approach to obtain optimal outcomes.

Keywords Rotary turning · Total energy consumed · Total machining time · NSPSO

1 Introduction

The rotary turning operation using a circular insert is an effective manufacturing solution to machine hardened steels. The round insert is continuously rotated around its axis, which is employed to remove the material. This process can be divided into two kinds, including the actively driven rotary turning (ADRT) and self-propelled rotary tool (SPRT) turning processes. For the ADRT process, the motion of the round insert is conducted using an external motor, as shown in Fig. 1. The rotary turning operation provides a rest period, which has a significant contribution to minimizing machining temperature, longer tool life, and higher productivity. Additionally, the machined quality is also improved, as compared to the fixed turning. Therefore, the rotary turning process has great potential to replace the traditional approaches, such as grinding, hard turning, and polishing operations [1].

The selection of optimal factors for improving machining performances of various rotary turning operations has been considered by many researchers. The traditional objectives are the cutting temperature, tool wear, average roughness, and turning force. Armarego et al. [2] analyzed the influences of the cutting speed, feed rate, and depth of cut on the turning temperature of the rotary and fixed turnings. The results indicated that the temperature produced by the rotary turning was evenly distributed and decreased by 50 °C, as compared to the fixed turning. Dessoly et al. [3] investigated the influences of the cutting speed, depth of cut, different workpieces, and various inserts (carbide, coated carbide, and ceramics) on the tool wear and the formation of the chip. These authors stated that the tool wear was only observed on the flank surface and the range of the cutting speed could be increased with

✉ Trung-Thanh Nguyen
trungthanhk21@mta.edu.vn;
trungthanhnguyen@lqdtu.edu.vn

[1] Faculty of Mechanical Engineering, Le Quy Don Technical University, 236 Hoang Quoc Viet, Ha Noi 100000, Viet Nam

Published online: 19 March 2021

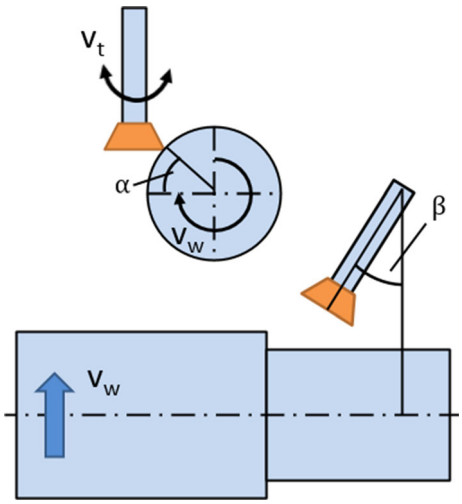

Fig. 1 Principle of the actively driven rotary turning process

the rotary turning. The analytical model of the tool wear for the rotary turning of the hardened AISI 4340 steel was proposed by Kishawy et al. [4]. The outcomes revealed that the designed models could be effectively employed to forecast the tool wear. Kishawy analyzed the characteristics of the tool wear, average roughness, and surface topography of the aerospace workpieces under the variations of the machining parameters [5]. These authors indicated that the flank wear was evenly distributed in the rotary insert, while the average roughness and cutting force were lower than the conventional approach. Wang et al. [6] applied a neural network to develop the approximate models of the three force components regarding the cutting speed, depth of cut, feed rate, and inclined angle. The small deviations compared with the experimental results revealed that the proposed models are adequate. Li and Kishawy [7] used the Oxley algorithm to construct the machining force model for the SPRT turning, in which the characteristics of the frictional coefficient and tool wear were analyzed with the aid of the experiments. The findings showed that the precision of the developed force model was satisfactory. Ezugwu et al. [8] emphasized that the rotary turning could provide longer tool life, lower machining forces, and higher material removal rate for machining aero-engine alloys. The approximate models of the average roughness and material removal rate for the rotary turning of hardened steel were developed by Rao et al. [9]. These authors presented that the average roughness was decreased to 1.49 μm, while the material removal rate did not change.

Teimouri et al. [10] developed the empirical models of the machining force and average roughness in terms of the cutting speed, tool rotary speed, and feed rate for the ADRT and ultrasonic vibration assisted-rotary turning (UART) processes of the aluminum alloy. The obtained findings indicated that the UART process could provide lower cutting force and average roughness, as compared to the ADRT operation. Lotfi et al. [11] proposed a simulation model to assess the behaviors of the tool wear and cutting temperature in traditional, rotary, and UART operations. The machining experiments were performed to analyze the impacts of the vibrational motion on the wear, heat generation, average roughness, and cutting force, respectively. The findings revealed that average roughness and cutting force were decreased around 50%, as compared to the traditional approach. Shasahara et al. [12] emphasized that the cutting temperature and flank wear could be decreased with the aid of the oil mist. Moreover, these authors emphasized that the values of the cutting temperature and tool wear of the ADRT turning were lower than that of the fixed tool. A self-propelled rotary face milling tool was developed by Jegaraj et al. [13] to improve the production rate in the rough machining. The empirical models of the milling force components were proposed in terms of the cutting speed, feed rate, depth of cut, and inclination angle. The small errors between the experimental and predictive results indicated that the regression models are significant. Amini and Teimouri [14] executed an attempt to minimize the machining force and average roughness of the UART operation of the aluminum alloy. The authors stated that the optimal values of the cutting velocity, tool speed, feed rate, and depth of cut were 4 m/min, 220 RPM, 0.08 mm/rev., and 0.3 mm, respectively. The impacts of the tool rotational speed and direction on the cutting forces, temperature, and chip formation for the ADRT operation of the carbon steel were explored by Suryadiwansa et al. [15]. The findings revealed that the cutting temperature was decreased with an increment in the tool speed, while the force components were increased. Similarly, the influences of the workpiece and tool speed on the cutting temperature for the ADRT operation of the stainless steel and Inconel were investigated by Hosokawa et al. [16]. The authors stated that lower workpiece speed and/or higher tool speed caused a reduction in the cutting temperature.

Recently, resolving the relations between energy consumption, machined quality, and productivity has been addressed in the published works. Nguyen applied the adaptive neuro-fuzzy inference system (ANFIS) to render the relations between the energy consumption, average roughness, and machining rate in terms of the inclination angle, depth of cut, feed rate, and cutting speed for the SPRT turning [17]. The authors emphasized that the energy used and average roughness were reduced by 50.29% and 19.77%, while the machining rate was improved by 33.16%, respectively, at the optimal solution. The assessment of the sustainable indicators, including energy efficiency, turning cost, average roughness, and operational safety for the SPRT process were conducted by Nguyen et al. [18], in which the neighborhood cultivation genetic

algorithm (NCGA) was applied to identify the optimal factors. As a result, the improvement in energy efficiency was 8.91%, while the average roughness and cost were decreased by 20.00% and 14.75%, respectively, at the optimal point.

As a result, optimizations of different SPRT processes for improving the machining responses have been thoroughly investigated by former researchers. The conventional responses are the tool wear, average roughness, cutting force, production rate, energy consumption, and energy efficiency. Unfortunately, enhancing the technical performances of the ADRT process has got less attention. The analysis of the total energy consumption and machining time has not been performed for the ADRT operation. Additionally, the experimental approach was intensively employed to investigate the turning characteristics, which requires huge efforts and expensive costs.

In this investigation, the actively driven rotary turning (ADRT) process of the mold material namely SKD11 has been addressed to decrease the total energy consumption and machining time, while the average roughness is considered as a constraint. Firstly, the active driven rotary tool is designed and fabricated. The specimen labeled SKD11 is employed due to wide applications in the mold, marine, and automotive industries. An analytical approach is used instead of the experimental method to develop comprehensive models of the total energy consumption and machining time. The non-dominated sorting particle swarm optimization (NSPSO) is applied to generate feasible solutions. The weight principle component analysis (WPCA) is employed to select the weight values of each turning response. The Technique for Order of Preference by Similarity to Ideal Solution (TOPSIS) is applied to select the best optimal point.

2 Optimization framework

2.1 Optimization issue

The literature revealed that the machining conditions considered are the characteristics of the rotary insert (diameter, normal rake angle, and materials), the process parameters (inclination angle, tool rotational speed, workpiece speed, depth of cut, and feed rate), lubrication characteristics (dry machining, minimum quantity lubrication-MQL, flood lubrication, and cryogenic machining), and the workpiece materials. The affecting factors most likely to influence energy consumed, quality, and machining time are shown in Fig. 2 with the aid of the Ishikawa diagram.

In the current work, the characteristics of the round insert and workpiece are listed as stable conditions. All tests are performed in the flood condition and the inclination angle of 0° is used. Therefore, the tool rotational speed, workpiece speed, depth of cut, and feed rate are considered as the optimizing inputs.

The considered factors and their levels are presented in Table 1. The parameter ranges are selected based on the characteristics of the machined tool employed as well as rotary insert and verified with the literature review. The turning trials at the highest levels are conducted to ensure that the power consumed is less than the maximum power.

In this work, two turning responses, including the total energy consumed and total machining time, are simultaneously optimized using an integrative approach with the constraint of the average roughness. The value of the average roughness is predefined as a constant for a specific machining purpose.

Therefore, the optimization issue can be expressed as:

Find $X = [v_t, a, f, \text{and } v_w]$.

Minimizing total energy consumption and total machining time.

Constraints: $40 \leq v_t \leq 100$ (m/min); $0.20 \leq a \leq 1.00$ (mm); $0.08 \leq f \leq 0.5$ (mm/rev.);

$80 \leq v_w \leq 200$.

$R_a \leq R_{a\ \text{upper}}$.

2.2 Optimization framework

The optimization approach includes the following steps.

Step 1: The comprehensive models of the total energy consumed and total machining time are then developed with respect to process parameters using the analytical method [19, 20].

The total machining time (T_{total}) is expressed as:

$$T_{\text{total}} = t_o + t_{sb} + t_{air} + t_c + t_{tc} \tag{1}$$

where t_o the start-up time; t_{sb} the standby time; t_{air} the air-turning; t_c the turning time; t_{tc} the tool change time.

Practically, the start-up, standby, and tool change times can be considered as constants.

The air-turning time (t_{air}) is calculated as:

$$t_{air} = h_1 L + h_2 \tag{2}$$

where h_1 tool travel time; h_2 tool depart time; L total machining length.

The turning time (t_c) is calculated as [21]:

$$t_c = \frac{\text{MRV}}{\text{MRR}}\left(1 + \frac{t_{tc}}{T}\right) \tag{3}$$

where MRV the material removal volume; MRR the material removal rate; T the tool life.

The values of the MRV and MRR are computed as:

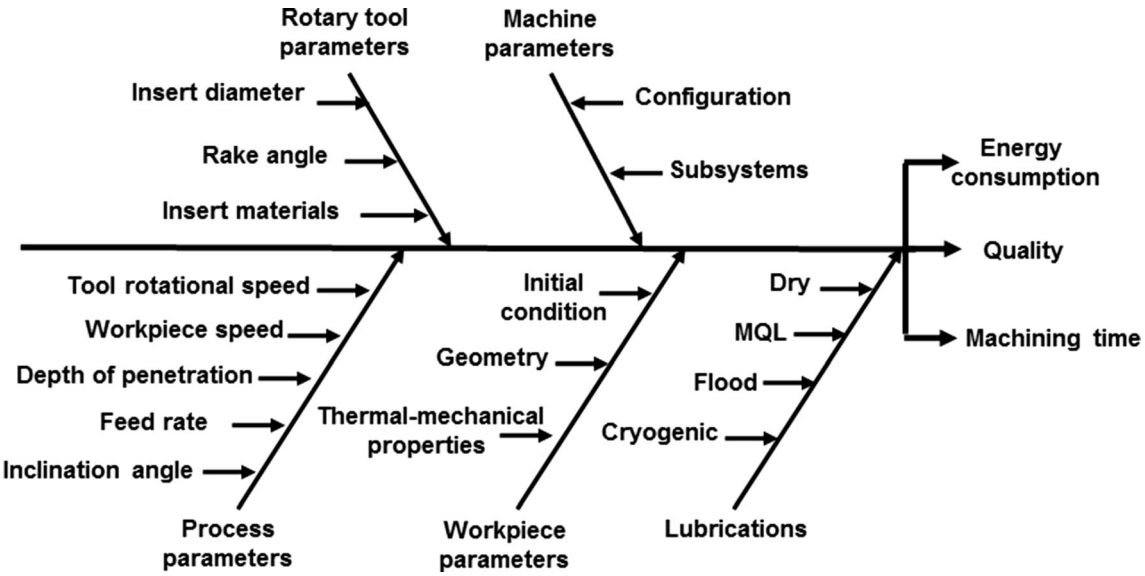

Fig. 2 The affecting parameters on the turning responses

Table 1 Process parameters and their ranges

Parameters	Symbol	Unit	Ranges
Tool speed	v_t	m/min	40–100
Depth of cut	a	Mm	0.20–1.00
Feed rate	f	mm/rev	0.08–0.50
Workpiece speed	v_w	m/min	80–200

$$\mathrm{MRV} = \frac{\pi DLa}{1000} \tag{4}$$

$$MRR = \frac{vfa}{60} \tag{5}$$

where D the turning diameter; L the turning length; v the resulting cutting speed.

The value of the resulting cutting speed is computed as:

$$v = [(v_w \cos\beta)^2 + (V_t + v_w \sin\beta)^2]^{1/2} \tag{6}$$

The tool life equation can be extended to include process parameters for the turning operation, which is computed as [22]:

$$T = 60\frac{A^{\alpha}}{v^{\alpha} f^{\beta} a^{\gamma}} \tag{7}$$

where A the coefficient related to the cutting conditions; α, β, and γ positive constant parameters depending on the tool material and workpiece.

Fortunately, the tool life was enhanced by 300% with the aid of the 5% water-based cutting fluid, as compared to the dry cutting environment [23]. Additionally, the positive impacts of the cutting fluid on the tool wear and average roughness were recognized [24]. Therefore, the coefficient related to the reduction in the tool wear (k_T) using the cutting fluid is taken into account the calculated value of the tool wear, which is shown as:

$$T = 60\frac{A^{\alpha}}{k_T v^{\alpha} f^{\beta} a^{\gamma}} \tag{8}$$

Thus, the total machining time (t_{total}) is calculated as:

$$t_{\mathrm{total}} = t_o + t_{sb} + h_1 L + h_2 + \frac{\mathrm{MRV}}{\mathrm{MRR}}\left(1 + \frac{t_{tc}}{T}\right) + t_{tc} \tag{9}$$

The total energy consumed in the turning process can be divided into two primary components, including the direct energy consumption and indirect energy consumption. The direct energy consumption is the electrical energy consumed by the machine tool during the turning process, which is used to operate the machine components such as the spindle, feed system, and auxiliary parts.

As shown in Fig. 3, the direct energy consumed (E_{direct}) in the ADRT process can be divided into the start-up energy (E_o), the standby energy (E_{sb}), transition energy for the spindle acceleration/deceleration state (E_{ts}), air-turning energy (E_{air}), turning energy (E_c), and tool change energy (Etc). The indirect energy consumption (E_{direct}) includes the energy footprint of the rotary turning tool (E_{ft}) and cutting fluid (E_{ff}).

Thus, the total energy model can be expressed as:

$$E_{\mathrm{total}} = E_o + E_{sb} + E_{ts} + E_{air} + E_c + + E_{tc} + E_{ft} + E_{ff} \tag{10}$$

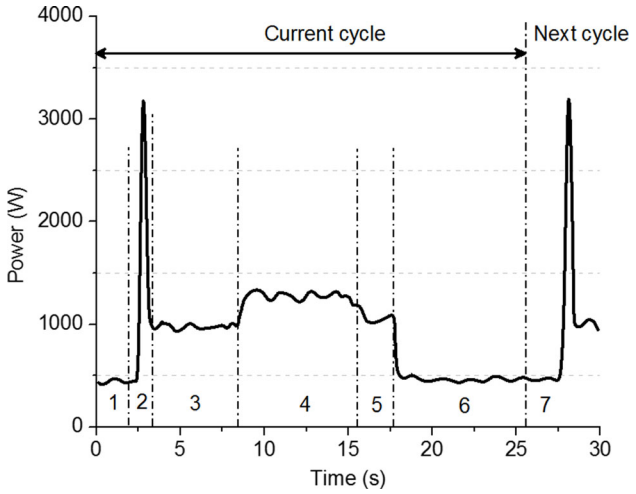

Fig. 3 The power profile of the turning operation

Practically, the energy consumed in the start-up and standby states a can be directly measured by experiments. Therefore, the start-up energy is considered as a constant.

The energy consumed in the standby state (E_{sb}) is calculated as:

$$E_{sb} = P_{sb} \times t_{sb} \tag{11}$$

where P_{sb} denotes the power consumed in the standby state.

The energy consumed in the transition state (E_{ts}) is expressed as:

$$E_{ts} = x_1 v^2 + x_2 v + x_3 \tag{12}$$

where x_i presents the experimental coefficients related to the characteristics of the machine tools.

The energy consumed in the air-cutting state (E_{air}) is calculated as:

$$\begin{aligned} E_{air} &= P_{air} \times t_{air} = (P_{sb} + P_{operational}) \times t_{air} \\ &= (P_{sb} + k_1 v + k_2) \times t_{air} \end{aligned} \tag{13}$$

where P_{air} the power consumed in the air-turning state; k_1 and k_2-the coefficients of the linear model.

The energy consumed in the turning state (E_c) is calculated as:

$$E_c = (\text{MRV} \times \text{SEC}) \tag{14}$$

$$\text{SEC} = (C_0 + \frac{C_1}{\text{MRR}}) \tag{15}$$

where C_0 and C_1 present the experimental coefficients to be determined.

The energy consumed of the tool change (Etc) is computed as:

$$E_{tc} = P_{sb} \times t_{tc}\left(\frac{t_c}{T}\right) \tag{16}$$

The energy footprint of the turning tool (E_{ft}) is calculated as:

$$E_{fp} = P_t\left(\frac{t_c}{T}\right) \tag{17}$$

where P_t is the tool energy per insert.

The energy footprint of the cutting fluid (E_{ff}) is calculated as:

$$E_{ff} = \frac{t_c V_A \eta \rho X_c}{T_{fl}} \tag{18}$$

where V_A is the consumption velocity of the cutting fluid; η the concentration of the cutting fluid; ρ the density of the cutting fluid; X_c the energy used to fabricate the cutting fluid; T_{fl} the cycle time of the cutting fluid used.

Step 2: The turning trials are performed to obtain the necessary data and identify the experimental coefficients [25].

Step 3: Generation of feasible solutions using non-dominated sorting particle swarm optimization (NSPSO) [26].

NSPSO is a powerful optimization technique to solve the trade-off analysis between the conflicting responses. It combines the advantages of the non-dominated sorting genetic algorithm (NSGA-II) and the particle swarm optimization (PSO), including the fast non-dominated sorting approach, crowding distance ranking, elitist strategy, mutation, selection operations, and the particle swarm searching. The hybrid algorithm includes the following steps, as shown in Fig. 4:

- Generating an initial population P (Population size = N) and velocity for each individual (agent or particle) in a feasible space. Setting the maximum speed v_i^{max} for a variable.
- Sorting the population based on the non-domination and crowding distance ranking.
- Performing the selection of the rank.
- Assigning the calculated rank of each individual to its non-domination level.
- Randomly choose one individual as gbest for N times from the non-dominated solutions, and modify each searching point using the following formula:

$$v_i^{k+1} = K\left[v_i^k + c_1 \times r_1 \times (\text{pbest}_i - s_i^k) + c_2 \times r_2 \times (\text{gbest} - s_i^k)\right] \tag{19}$$

$$s_i^{k+1} = s_i^k + v_i^{k+1} \tag{20}$$

where v_i^k and s_i^k present the velocity and position at the k generation, respectively. v_i^{k+1} and s_i^{k+1} denote the velocity and position at the $k + 1$ generation, respectively. r_1 and r_2 present a random number between (0, 1). c_1 and c_2 are two constant coefficients balancing the influence of the

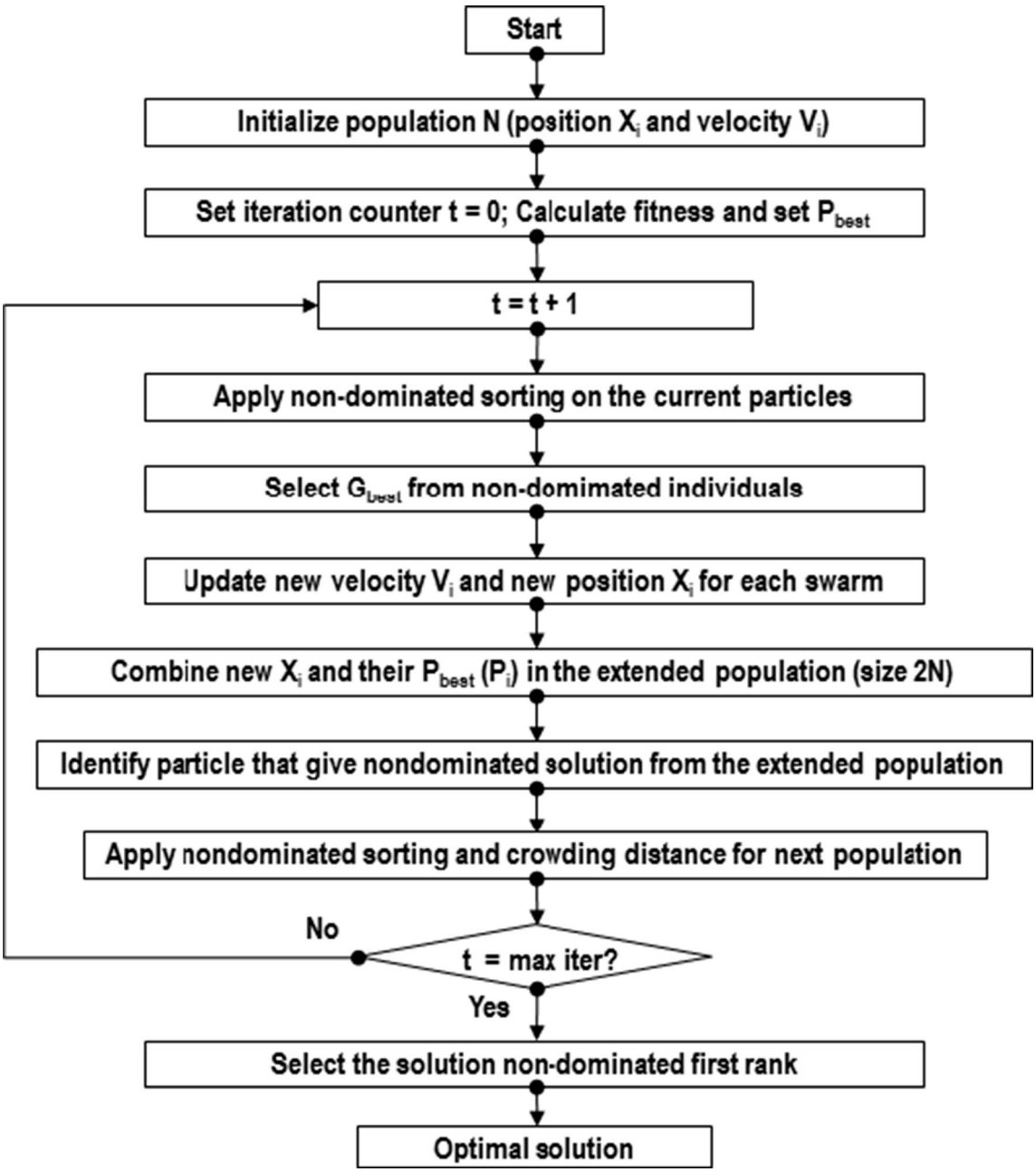

Fig. 4 Operating Principle of the NSPSO

best personal position of the particle $pbest_i$ and the best global position gbest.

- Performing mutation operation.
- Generating an extended population of size 2 *N* using a combination of the offspring and parent population.
- Sorting the extended population based on the non-domination operation. Filling the new population of size *N* with individuals from the sorting fronts.
- If the current rank of the new individual P_i^{k+1} is smaller than or equal to the parent in *R*, replacing the $pbest_i$ with the current individual. Otherwise keep the current $pbest_i$.
- Perform step (2) to (9) until the convergence is obtained.

Step 4: Determination of the weight of each turning response using the weightage principal component analysis (WPCA).

The normalization of the experimental data is conducted based on the optimization requirement.

For lower the better approach, the normalized data is computed as:

$$I^*(k) = \frac{\min I_i(m)}{I_i(m)} \tag{21}$$

For higher the better approach, the normalized data is computed as:

$$I^*(k) = \frac{I_i(m)}{\max I_i(m)} \tag{22}$$

In the current work, the weight value is directly calculated from the experimental data and it does not depend on the operator's choice. The important role of the weight value is to objectively reflect the importance of each response. The weight calculated is assigned to each response when the optimization process performs.

The correlation coefficient is calculated as [27]:

$$S_{jl} = \left[\frac{\mathrm{Cov}(I_i(j), I_i(l))}{\sigma_{Ii}(j) \times \sigma_{Ii}(l)}\right] \tag{23}$$

where is $\mathrm{Cov}(I_i(j), I_i(l))$ the covariance of sequences $I_i(j)$ and $I_i(l)$; $\sigma_{Ii}(j)$ the standard deviation of sequences $I_i(j)$; $\sigma_{Ii}(l)$ the standard deviation of sequences $I_i(l)$.

The eigenvalues and consequent eigenvectors are calculated as:

$$(S - \lambda_k J_m) V_{ik} = 0 \tag{24}$$

where λ_k is the eigenvalues; V_{ik} the eigenvectors; J_m the identity matrix, respectively.

The major principal coefficient is calculated as:

$$PC_m = \sum_{i=1}^{n} I_m(i) \times V_{ik} \tag{25}$$

Step 5: Determination of the best solution using the TOPSIS [28].

The weighted value of each response is calculated as:

$$V_{ij} = I_i w_i \tag{26}$$

where w_i is the weight value calculated; V_{ij} the weighted response.

The positive ideal solution (S^+) and the negative ideal solution (S^-) are determined as:

$$V^+ = (v_1^+, v_2^+, v_3^+, \ldots, v_n^+) \quad \text{maximum values} \tag{27}$$

$$V^- = (v_1^-, v_2^-, v_3^-, \ldots, v_n^-) \quad \text{minimum values} \tag{28}$$

$$S_i^+ = \sqrt{\sum_{j=1}^{m} (v_{ij} - v_j^+)^2} \tag{29}$$

$$S_i^- = \sqrt{\sum_{j=1}^{m} (v_{ij} - v_j^-)^2} \tag{30}$$

The best solution is determined based on the highest desirability (D) value. The desirability value is calculated as:

$$D = \frac{S_i^-}{S_i^+ + S_i^-} \tag{31}$$

3 Experiment and modeling

3.1 Experimental detail

The steel bar labeled SKD11 is selected as the workpiece in the current work due to widely applications in the mold, automotive, and marine industries. The characteristics of each workpiece for the turning experiment are depicted in Table 2. The chemical compositions of the SKD11 are shown in Table 3. The machining length of 75 mm is applied to three machining segments (Fig. 5).

The carbide inserts having 15° rake angle produced by MISUBISHI are used in all turning trials. The outside diameter, inside diameter, and thickness of the round insert are 16 mm, 5.6 mm, and 6.4 mm, respectively. The hardness of the employed insert is around 91 HRC. The tool shank is fabricated using a mold steel labeled SKD61. The hardness of the tool shank is around 80 HRC.

All the turning trials are performed on a CNC lathe labeled EMCO MAXXTURN 45, which has four axes to perform the turning and milling functions. The maximum power and speed of the main spindle are 12 kW and 6300 RPM, respectively. The maximum power and speed of the tool spindle are 6 kW and 4000 RPM, respectively. The

Table 2 The characteristics of each workpiece

Total length of each workpiece	Mm	250
Diameter	Mm	40
Number of segments		3
The length of each segment	Mm	25
Hardness	HRC	50

Table 3 Chemical compositions of the SKD11

C (%)	Si (%)	Mn (%)	*P* (%)	*S* (%)	Cr (%)	Mo (%)	*V* (%)
1.40	0.40	0.60	0.03	0.03	11.0	0.80	0.30

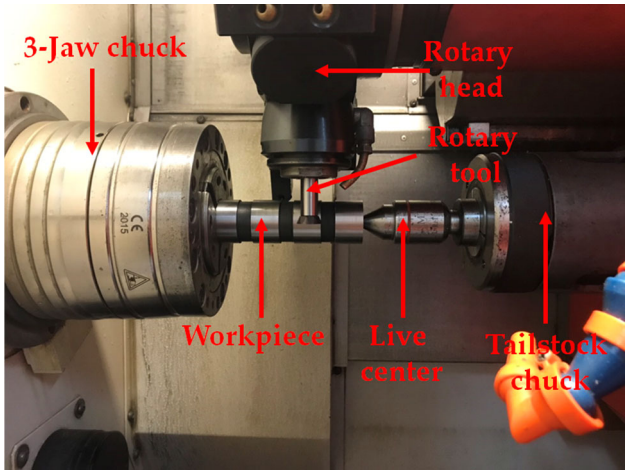

Fig. 5 Experiments of the rotary turning

specimen is clamped by the chuck. The live center is used to ensure machining rigidity. The power consumed of the actively driven rotary turning is recorded using a power sensor.

3.2 Development of regression models for the energy consumed in the transition state, power in the air cutting state, and energy consumed in the cutting state

In the current work, the design of experiment entitled the full factorial is employed to generate the matrix table with the parameter combination. Three levels of three process parameters (i.e. v, f, and a) are used and total twenty-seven tests are needed for this experiment, as shown in Table 4. The response surface method is applied to develop the regression models of the technical performances.

The regression models for the energy consumed in the transition state, power in the air cutting state, and energy consumed in the cutting state were developed using the regression method (Table 5). The values of the coefficient determinations, including the R^2, adjusted R^2, and predicted R^2 indicated that the fidelity of the proposed models is acceptable.

The average roughness mainly depends on the feed rate and nose radius. As mentioned in the previous section, the cutting fluid helps to minimize the average roughness [24]. Therefore, the coefficient related to the reduction in the average roughness (k_{AR}) using the cutting fluid is taken into account the calculated value of the feed rate, which is shown as:

$$f_{\max} = \sqrt{\frac{R_{a\max} \times r_{\varepsilon}}{32.1 \times k_{AR}}} \tag{32}$$

where $R_{a\max}$ is the maximum average roughness; r_{ε} the nose radius of the insert; k_{AR} the coefficient related to the reduction in the average roughness using the cutting fluid.

The coefficients for the ADRT process are shown in Table 6.

In this work, the water-based soluble oil is utilized as the cutting fluid. The coefficients for the water-based soluble oil are presented in Table 7 [29].

In the current work, an average roughness of 6.3 μm is employed. Therefore, the maximum feed rate of 0.44 mm/rev. is applied in the optimization process.

4 Results and discussions

The developed models of the total energy consumption and machining time are used to identify optimal parameters with the aid of the NSPSO. The operating parameters of the NSPSO are shown in Table 8.

The Pareto fronts showing the global relationship between the total energy consumed and total machining time generated by NSPSO are shown in Fig. 6. It can be stated that the trends of the target functions are contradictory. The minimization of the total energy leads to an increment in the total machining time and versus. Therefore, it is tough to select the optimal point, which can satisfy all objectives.

Two typical solutions, including points 1 and 2, are chosen to evaluate the turning performances in comparison with the initial values (Table 9). For the first point, the total energy consumption increases, as compared to the initial values, this cannot consider as a technical solution. For the second solution, the total energy consumed and machining time simultaneously decrease.

The similar relationships between the machining responses considered (the average roughness, energy efficiency, cost, and material removal rate) can be found in the works of [9, 18]. All technological performances tend to conflict with each other. For the work of [9], the material removal rate has conflict with the average roughness. Similarly, the average roughness has contradictory impact with the energy efficiency and cost in the work of [18].

The feasible solutions produced by NSPSO are shown in Table 10.

Table 4 Experimental data during the transition state, air-turning state, and turning state

No.	v (m/min)	f (mm/rev.)	a (mm)	MRR (cm^3/s)	EC_{ts} (kJ)	$P_{operational}$ (kW)	SEC (kJ/cm^3)
1	0.2	0.08	89.44	0.0239	0.6126	0.28448	30.4997
2	0.2	0.08	152.32	0.0406	0.9031	0.45008	18.4877
3	0.2	0.08	223.61	0.0596	1.4806	0.63829	13.0406
4	0.2	0.29	89.44	0.0865	0.6022	0.28512	9.4290
5	0.2	0.29	152.32	0.1472	0.9013	0.45181	6.1153
6	0.2	0.29	223.61	0.2162	1.4828	0.63892	4.6126
7	0.2	0.50	89.44	0.1491	0.6047	0.28542	6.0576
8	0.2	0.50	152.32	0.2539	0.9034	0.45028	4.1357
9	0.2	0.50	223.61	0.3727	1.4821	0.63906	3.2642
10	0.6	0.08	89.44	0.0716	0.6039	0.28478	11.1012
11	0.6	0.08	152.32	0.1219	0.9046	0.45080	7.0972
12	0.6	0.08	223.61	0.1789	1.4818	0.63952	5.2815
13	0.6	0.29	89.44	0.2594	0.6142	0.28402	4.0777
14	0.6	0.29	152.32	0.4417	0.9051	0.45124	2.9731
15	0.6	0.29	223.61	0.6485	1.4809	0.63846	2.4722
16	0.6	0.50	89.44	0.4472	0.6064	0.28462	2.9539
17	0.6	0.50	152.32	0.7616	0.9048	0.45142	2.3132
18	0.6	0.50	223.61	1.1181	1.4838	0.63907	2.0227
19	1.0	0.08	89.44	0.1193	0.6132	0.28525	7.2215
20	1.0	0.08	152.32	0.2031	0.9038	0.45192	4.8191
21	1.0	0.08	223.61	0.2981	1.4854	0.63884	3.7297
22	1.0	0.29	89.44	0.4323	0.6128	0.28468	3.0074
23	1.0	0.29	152.32	0.7362	0.9129	0.45132	2.3447
24	1.0	0.29	223.61	1.0808	1.4812	0.63846	2.0441
25	1.0	0.50	89.44	0.7453	0.6048	0.28558	2.3331
26	1.0	0.50	152.32	1.2693	0.9025	0.45042	1.9487
27	1.0	0.50	223.61	1.8634	1.4826	0.63784	1.7744

Table 5 Regression models of the energy consumed in the transition state, the power in the air cutting state, and the energy consumed in the cutting state

No.	Regression model	R^2	Adjusted R^2	Predicted R^2
1	$EC_{ts} = 0.00002588v^2 - 0.001543v + 0.5346$	0.9865	0.9848	0.9386
2	$P_{operational} = 0.00264v + 0.04896$	0.9906	0.9872	0.9685
2	$SEC = 1.402 + 0.694/MRR$	0.9873	0.9764	0.9586

Table 6 Coefficients for the ADRT process

P_o	P_{sb}	t_o	t_{sb}	h_1	h_2	L	t_{tc}	A	α	β	γ	k_T	k_{SR}
kW	kW	s	s	s/mm	S	mm	S						
0.52	0.78	2	6	42×10^{-3}	6	78	12	900	2.13	1	0.3	3	0.8

Table 7 Coefficients for the cutting fluid

X_c J/g	P g/cm^3	V_a l/s	T_{fl} s	η %
42,287	0.92	0.02	2.88×10^5	5

In this work, the eigenvalues, proportions, and eigenvectors of the machining responses were calculated with the aid of the Minitab software. The weight value of each response is computed based on the eigenvectors. Table 11 lists eigenvalues and proportion for each principal component. The first and second components account for 94.28% and 0.41%, respectively. Therefore, the contribution is calculated using the squares of the first eigenvector. As a result, the weight values of the total energy

Table 8 Setting parameters of the NSPSO

Parameter	Value
The number of particles	100
Maximum iterations	100
Weighting factor c_1	2
Weighting factor c_2	2
Mutation rate	0.5
Crossover probability	0.9

consumption and machining time are 0.59 and 0.41, respectively (Table 12).

The positive, negative, and desirability values are shown in Table 13. The highest desirability value is obtained at the experimental number 30. As a result, the optimum values of the tool speed, depth of cut, feed rate, and workpiece speed are 78 m/min, 0.21 mm, 0.44 mm/rev., and 999 m/min, respectively. The reductions of the total energy consumption and machining time are 16.99% and 17.78%, respectively, as compared to the initial values (Table 14).

To confirm the correctness of the optimization result, a confirmatory experiment is executed at the optimal solution. The deviations of the total energy consumed and total machining time are 1.5% and 1.4%, respectively (Table 15). The errors of less than 5.0% are acceptable in optimization engineering, which indicates the truth of the selected solution.

As mentioned in the former section, the actively driven turning operation provides various advantages, including lower machining temperature as well as average roughness, longer tool life, and higher productivity, as compared to the fix turning. This process has great potential to replace the traditional approaches, such as grinding, hard turning, and polishing operations for machining hardened steels. Therefore, the selection of optimal parameters for the actively driven turning operation in terms of the energy-saving, production rate, and machining quality is in urgent demand. In this investigation, a multi-response optimization of the actively driven rotary turning process has been addressed to decrease the total energy consumed and total machining time with the constraint value of the average roughness. The current work did consider not only the social impact (average roughness) but also the economic

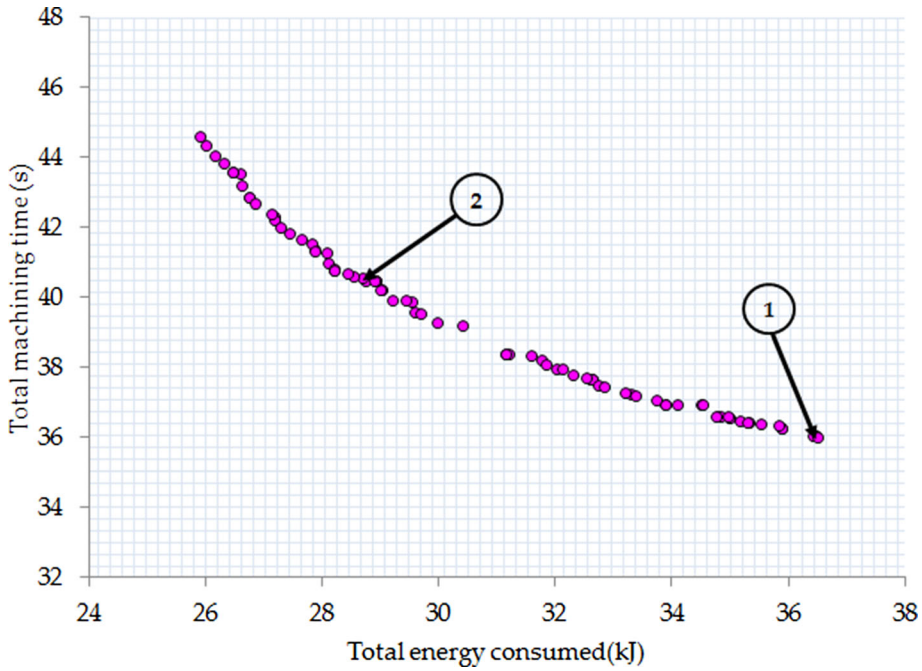

Fig. 6 Total machining time and total energy consumed

Table 9 Comparisons among feasible solutions

Method	v_t (m/min)	a_p (mm)	f (mm/rev.)	v_w (m/min)	E_{total} (kJ)	T_{total} (s)
Common values used	60	0.50	0.26	100	34.36	49.42
Point 1	98	0.44	0.21	197	36.55	36.12
Point 2	78	0.21	0.44	99	28.52	40.63

Table 10 Feasible solutions generated by NSPSO

No.	v_t (m/min)	a (mm)	f (mm/rev.)	v_w (m/min)	E_{total} (kJ)	T_{total} (s)
1	83	0.21	0.44	195	35.71	36.41
2	96	0.21	0.44	165	33.95	37.09
3	81	0.21	0.44	100	28.83	40.40
4	95	0.21	0.44	103	29.66	39.58
5	81	0.21	0.44	148	32.10	37.96
6	79	0.21	0.44	176	34.10	36.98
7	81	0.21	0.44	165	33.28	37.34
8	72	0.21	0.43	101	28.40	41.01
9	98	0.21	0.44	131	31.62	38.20
10	83	0.21	0.44	106	29.28	39.99
11	68	0.21	0.44	83	27.24	42.42
12	81	0.21	0.44	183	34.71	36.77
13	88	0.21	0.44	164	33.50	37.22
14	95	0.22	0.44	129	31.53	38.38
15	91	0.20	0.44	200	36.25	36.13
16	81	0.21	0.44	150	32.29	37.85
17	95	0.20	0.44	110	29.96	39.27
18	76	0.21	0.44	84	27.51	41.87
19	78	0.21	0.44	178	34.33	36.93
20	81	0.20	0.44	147	31.84	37.99
21	68	0.20	0.44	162	32.52	37.63
22	84	0.20	0.44	190	35.21	36.47
23	81	0.21	0.44	86	27.92	41.34
24	78	0.21	0.44	106	28.99	40.25
25	80	0.20	0.44	126	30.35	38.99
26	79	0.20	0.44	162	32.96	37.44
27	92	0.21	0.44	105	29.58	39.63
28	76	0.21	0.44	83	27.49	41.89
29	88	0.21	0.44	129	30.99	38.59
30	78	0.21	0.44	99	28.52	40.63
31	78	0.21	0.44	182	34.48	36.79
32	90	0.20	0.44	106	29.40	39.74
33	78	0.21	0.44	86	27.84	41.57
34	68	0.21	0.44	83	27.12	42.46

Table 11 Eigenvalues and proportions of the principal components

Principal component	Eigenvalues	Proportion (%)
First	1.8856	94.28
Second	0.1144	5.72

Table 12 Eigenvectors and contributions for the principal components

Characteristics	Eigenvectors		Weight value
	PC1	PC2	
E_{total}	−0.847	−0.787	0.59
T_{total}	0.707	−0.767	0.41

indicator (machining time) and environmental dimension (energy consumption). A specific case study of the actively driven rotary turning of SKD 11 steel was successfully executed to decrease the total energy consumed and total machining time. The scientific outcomes of the current work can be listed as follows:

The trade-off relation between the total energy consumed and total machining time with the constraint of the average roughness is solved by means of the optimization of process parameters. Minimizing energy consumed and

Table 13 Desirability values

No.	$S+$	$S-$	D
1	5.0693	2.5017	0.3304
2	4.0496	2.5904	0.3901
3	2.0247	4.4602	0.6878
4	2.0647	4.0649	0.6632
5	3.0318	3.0709	0.5032
6	4.1312	2.5842	0.3848
7	3.6720	2.7365	0.4270
8	2.1415	4.6719	0.6857
9	2.7860	3.2485	0.5383
10	2.0350	4.2375	0.6756
11	2.5833	5.3178	0.6730
12	4.4847	2.5080	0.3587
13	3.7890	2.6978	0.4159
14	2.7627	3.2511	0.5406
15	5.3868	2.5959	0.3252
16	3.1311	3.0084	0.4900
17	2.1160	3.9367	0.6504
18	2.3680	5.1676	0.6858
19	4.2675	2.5372	0.3729
20	2.8866	3.1881	0.5248
21	3.2445	2.9645	0.4775
22	4.7783	2.5335	0.3465
23	2.1925	4.9395	0.6926
24	2.0187	4.3833	0.6847
25	2.2407	3.7626	0.6268
26	3.4862	2.8342	0.4484
27	2.0433	4.1061	0.6677
28	2.3768	5.1775	0.6854
29	2.4975	3.4890	0.5828
30	2.0250	4.6239	0.6954
31	4.3520	2.5507	0.3695
32	2.0044	4.1943	0.6766
33	2.2760	4.9755	0.6861
34	2.5997	5.3889	0.6746

machining time with the constraint of the average roughness is a reliable approach, as compared to the simultaneous optimization of three turning responses.

The analytical models presenting the relationships between the process parameters and the total energy consumption and total machining time can be applied to forecast the machining responses in industrial applications with acceptable precision. These developed models are effectively employed to reduce experimental costs and human efforts.

The Pareto front could significantly help machine operators to determine proper parameters for saving energy consumed and machining time with the predefined constraint of the average roughness. The appropriate selection of process parameters can decrease machining costs, time, operator skills, and efforts.

The proposed approach using the analytical method, NSPSO, WPCA, TOPSIS can be used to develop comprehensive correlation models of turning performances and to effectively select the optimal solution, as compared to the trial method and operator experience. This optimizing technique is powerful and can be applied to different rotary turning operations.

The findings and outcomes in this investigation can be effectively employed in future studies for sustainable design as well as manufacturing. The obtained data can be directly applied in expert systems for the rotary turning operation in industrial applications.

5 Conclusions

In the current work, an attempt has been made to optimize machining conditions of the actively driven rotary turning for a mold material for reducing total energy consumption and machining time. The average roughness is predefined as the constraint. The analytical approach was employed to develop comprehensive models of total energy

Table 14 The optimal values of the process parameters and responses

Method	v_t (m/min)	a_p (mm)	f (mm/rev.)	v_w (m/min)	E_{total} (kJ)	T_{total} (s)
Common values	60	0.50	0.26	100	34.36	49.42
Optimal values	78	0.21	0.44	99	28.52	40.63
Improvement (%)					−16.99	−17.78

Table 15 The confirmatory results at the optimal solution

Method	v_t (m/min)	a_p (mm)	f (mm/rev.)	v_w (m/min)	E_{total} (kJ)	T_{total} (s)
Optimal values	78	0.21	0.44	99	28.52	40.63
Experiment	78	0.21	0.44	99	28.96	40.06
Improvement (%)					−1.52	1.40

consumption and machining time. The NSPSO was used to yield feasible points. The WPCA and TOPSIS were employed to select the weight value of each turning response and determine the best optimal point. The finding can be listed as bellows:

1. The analytical models of total energy consumption and machining time are adequate and significant. The proposed models can be employed to predict the values of the technical performances with sufficient accuracy.
2. As shown in the optimal setting generated by NSPSO-WPCA-TOPSIS, the optimal parameters of the tool rotational speed, depth of cut, feed rate, and workpiece speed are 78 m/min, 0.21 mm, 0.44 mm/rev., and 99 m/min, respectively. The total energy consumption and machining time are decreased by 16.99% and 17.78%, respectively, as compared to common values used.
3. The optimization investigation of the actively driven rotary turning, in which the energy consumed and machining time are responses and average roughness is predefined, is practical and reliable, as compared to the single objective and simultaneously optimizing three responses.
4. The proposed optimization technique can be considered as a powerful approach to select the optimal values of process parameters and technological performances in the rotary turning process and save operator efforts as well as experimental costs. The optimization outcomes are efficiently determined with the support of the optimization method instead of employing the human experience and/or manual handbook.
5. The development of an actively driven rotary turning, including the fabrication of the rotary tool and selection of optimal factors could be considered as a technical solution to enhance the machining efficiency and decrease environmental impacts for turning processes of hardened steels.
6. In this work, the average roughness value is primarily affected by the feed rate and nose radius. Practically, other factors, such as the depth of cut, tool rotational speed, and work speed have a significant influence on the formation of the average roughness. A comprehensive optimization considering more process parameters will be addressed in future works.

Funding This research is funded by Vietnam National Foundation for Science and Technology Development (NAFOSTED) under grant number 107.04 2020.02.

Declarations

Conflict of interest The authors declare no conflict of interest.

References

1. Armarego EJA, Karri V, Smith AJR (1994) Fundamental studies of driven and self-propelled rotary tool cutting processes-I. Theoretical investigation. Int J Mach Tools Manuf 34(6):785–801. https://doi.org/10.1016/0890-6955(94)90059-0
2. Dessoly V, Melkote SN, Lescalier C (2004) Modeling and verification of cutting tool temperatures in rotary tool turning of hardened steel. Int J Mach Tools Manuf 44(14):1463–1470. https://doi.org/10.1016/j.ijmachtools.2004.05.007
3. Kishawy HA, Wilcox J (2003) Tool wear and chip formation during hard turning with self-propelled rotary tools. Int J Mach Tools Manuf 43(4):433–439. https://doi.org/10.1016/s0890-6955(02)00239-0
4. Kishawy HA, Pang L, Balazinski M (2011) Modeling of tool wear during hard turning with self-propelled rotary tools. Int J Mech Sci 53(11):1015–1021. https://doi.org/10.1016/j.ijmecsci.2011.08.009
5. Kishawy HA, Becze CE, McIntosh DG (2004) Tool performance and attainable surface quality during the machining of aerospace alloys using self-propelled rotary tools. J Mater Process Technol 152(3):266–271. https://doi.org/10.1016/j.jmatprotec.2003.11.011
6. Wang SH, Zhu X, Li X, Turyagyenda G (2006) Prediction of cutting force for self-propelled rotary tool using artificial neural networks. J Mater Process Technol 180(1–3):23–29. https://doi.org/10.1016/j.jmatprotec.2006.04.123
7. Li L, Kishawy HA (2006) A model for cutting forces generated during machining with self-propelled rotary tools. Int J Mach Tools Manuf 46(12):1388–1394. https://doi.org/10.1016/j.ijmachtools.2005
8. Ezugwu EO (2007) Improvements in the machining of aero-engine alloys using self-propelled rotary tooling technique. J Mater Process Technol 185(1–3):60–71. https://doi.org/10.1016/j.jmatprotec.2006.03.112
9. Rao TB, Krishna AG, Katta RK (2015) Modeling and multiresponse optimization of machining performance while turning hardened steel with self-propelled rotary tool. Adv Manuf 3:84–95. https://doi.org/10.1007/s40436-014-0092-z
10. Teimouri R, Amini S, Mohagheghian N (2017) Experimental study and empirical analysis on effect of ultrasonic vibration during rotary turning of aluminum 7075 aerospace alloy. J Manuf Process 26:1–12. https://doi.org/10.1016/j.jmapro.2016.11.011
11. Lotfi M, Amini S, Aghaei M (2018) 3D FEM simulation of tool wear in ultrasonic assisted rotary turning. Ultrasonics 88:106–114. https://doi.org/10.1016/j.ultras.2018.03.013
12. Sasahara H, Satake K, Takahashi W, Goto W, Yamamoto H (2017) The Effect of oil mist supply on cutting point temperature and tool wear in driven rotary cutting. Precis Eng 48:158–163. https://doi.org/10.1016/j.precisioneng.2016.11.016
13. Jegaraj JJR, Raju C, Ramesh Kumar K, Rao C (2014) Experimental investigations and development of cutting force model for self-propelled rotary face milling cutter in machining of titanium alloy. Proc Inst Mech Eng B 228(9):1081–1089. https://doi.org/10.1177/0954405414522446
14. Amini S, Teimouri R (2017) Parametric study and multicharacteristic optimization of rotary turning process assisted by longitudinal ultrasonic vibration. Proc Inst Mech Eng B 231(5):978–991. https://doi.org/10.1177/0954408916651894

15. Suryadiwansa H, Toshiroh S, Toshimichi M (2008) Cutting Mechanics of turning with actively driven rotary tool. J Adv Mech Des Syst Manuf 2(4):579–586. https://doi.org/10.1299/jamdsm.2.579
16. Hosokawa A, Ueda T, Onishi R, Tanaka R, Furumoto T (2010) Turning of difficult-to-machine materials with actively driven rotary tool. CIRP Ann 59(1):89–92. https://doi.org/10.1016/j.cirp.2010.03.053
17. Nguyen TT (2020) An energy-efficient optimization of the hard turning using rotary tool. Neural Comput Appl. https://doi.org/10.1007/s00521-020-05149-2
18. Nguyen TT, Duong QD, Mia M (2020) Sustainability-based optimization of the rotary turning of the hardened steel. Metals 10:939. https://doi.org/10.3390/met10070939
19. Itu C, Öchsner A, Vlase S, Marin M (2019) Improved rigidity of composite circular plates through radial ribs. Proc Inst Mech Eng L 233(8):1585–1593. https://doi.org/10.1177/1464420718768049
20. Abd-Elaziz EM, Marin M, Othman MIA (2019) On the effect of Thomson and initial stress in a thermo-porous elastic solid under G–N electromagnetic theory. Symmetry 11:413. https://doi.org/10.3390/sym11030413
21. Lin W, Yu D, Zhang C, Zhang S, Tian Y, Liu S, Luo M (2017) Multi-objective optimization of machining parameters in multi-pass turning operations for low-carbon manufacturing. Proc Inst Mech Eng B 231(13):2372–2383. https://doi.org/10.1177/0954405416629098
22. Bagaber SA, Yusoff AR (2019) Energy and cost integration for multi-objective optimisation in a sustainable turning process. Measurement 136:795–810. https://doi.org/10.1016/j.measurement.2018.12.096
23. Popke H, Emmer T, Steffenhagen J (1999) Environmentally clean metal cutting processes – machining on the way to dry cutting. Proc Inst Mech Eng B 213(3):329–332. https://doi.org/10.1243/0954405991516813
24. Dhar NR, Kamruzzaman M (2007) Cutting temperature, tool wear, surface roughness and dimensional deviation in turning AISI-4037 steel under cryogenic condition. Int J Mach Tools Manuf 47(5):754–759. https://doi.org/10.1016/j.ijmachtools.2006.09.018
25. Mia M, Dhar NR (2019) Prediction and optimization by using SVR, RSM and GA in hard turning of tempered AISI 1060 steel under effective cooling condition. Neural Comput Appl 31:2349–2370. https://doi.org/10.1007/s00521-017-3192-4
26. Tang B, Xiang K, Pang M (2020) An integrated particle swarm optimization approach hybridizing a new self-adaptive particle swarm optimization with a modified differential evolution. Neural Comput Appl 32:4849–4883. https://doi.org/10.1007/s00521-018-3878-2
27. Nguyen TT, Mia M, Dang XP, Le CH, Michael SP (2020) Green machining for the dry milling process of stainless steel 304. Proc Inst Mech Eng B 234(5):881–899. https://doi.org/10.1177/0954405419888126
28. Ho L, Lin Y, Chen T (2020) A Pearson-like correlation-based TOPSIS method with interval-valued Pythagorean fuzzy uncertainty and its application to multiple criteria decision analysis of stroke rehabilitation treatments. Neural Comput Appl 32:8265–8295. https://doi.org/10.1007/s00521-019-04304-8
29. Chen X, Li C, Jin Y et al (2018) Optimization of cutting parameters with a sustainable consideration of electrical energy and embodied energy of materials. Int J Adv Manuf Technol 96:775–788. https://doi.org/10.1007/s00170-018-1647-0